







Article

Azimuthal Solar Synchronization and Aerodynamic Neuro-Optimization: An Empirical Study on Slime-Mold-Inspired Neural Networks for Solar UAV Range Optimization

Graheeth Hazare ¹, Mohamed Thariq Hameed Sultan ^{1,2,3,*}, Dariusz Mika ⁴, Farah Syazwani Shahar ¹, Grzegorz Skorulski ⁵, Marek Nowakowski ^{6,*}, Andriy Holovatyy ⁷, Ile Mircheski ⁸ and Wojciech Giernacki ⁹

- ¹ Department of Aerospace Engineering, Faculty of Engineering, Universiti Putra Malaysia, Serdang 43400, Selangor, Malaysia; graheeth@gmail.com (G.H.); farahsyazwani@upm.edu.my (F.S.S.)
 - ² Laboratory of Biocomposite Technology, Institute of Tropical Forest and Forest Product (INTROP), Universiti Putra Malaysia, Serdang 43400, Selangor, Malaysia
 - ³ Aerospace Malaysia Innovation Centre (944751-A), Prime Minister's Department, MIGHT Partnership Hub, Jalan Impact, Cyberjaya 63600, Selangor, Malaysia
 - ⁴ Institute of Technical Sciences and Aviation, The State School of Higher Education in Chelm, 22-100 Chelm, Poland; dmika@pwsz.chelm.pl
 - ⁵ Institute of Mechanical Engineering, Faculty of Mechanical Engineering, Bialystok University of Technology, 15-351 Bialystok, Poland; g.skorulski@pb.edu.pl
 - ⁶ Military Institute of Armoured and Automotive Technology, 05-070 Sulejowek, Poland
 - ⁷ Department of Computer-Aided Design Systems, Lviv Polytechnic National University, 79013 Lviv, Ukraine; andrii.i.holovatyy@lpnu.ua
 - ⁸ Faculty of Mechanical Engineering, SS Cyril and Methodius University in Skopje, 1000 Skopje, North Macedonia; ile.mircheski@mf.edu.mk
 - ⁹ Institute of Robotics and Machine Intelligence, Faculty of Control, Robotics and Electrical Engineering, Poznan University of Technology, 60-965 Poznan, Poland; wojciech.giernacki@put.poznan.pl
- * Correspondence: thariq@upm.edu.my (M.T.H.S.); marek.nowakowski@witpis.eu (M.N.)



Citation: Hazare, G.; Sultan, M.T.H.; Mika, D.; Shahar, F.S.; Skorulski, G.; Nowakowski, M.; Holovatyy, A.; Mircheski, I.; Giernacki, W. Azimuthal Solar Synchronization and Aerodynamic Neuro-Optimization: An Empirical Study on Slime-Mold-Inspired Neural Networks for Solar UAV Range Optimization. *Appl. Sci.* **2024**, *14*, 8265. <https://doi.org/10.3390/app14188265>

Academic Editor: Frede Blaabjerg

Received: 23 July 2024

Revised: 5 September 2024

Accepted: 11 September 2024

Published: 13 September 2024



Copyright: © 2024 by the authors. Licensee MDPI, Basel, Switzerland. This article is an open access article distributed under the terms and conditions of the Creative Commons Attribution (CC BY) license (<https://creativecommons.org/licenses/by/4.0/>).

Abstract: This study introduces a novel methodology for enhancing the efficiency of solar-powered unmanned aerial vehicles (UAVs) through azimuthal solar synchronization and aerodynamic neuro-optimization, leveraging the principles of slime mold neural networks. The objective is to broaden the operational capabilities of solar UAVs, enabling them to perform over extended ranges and in varied weather conditions. Our approach integrates a computational model of slime mold networks with a simulation environment to optimize both the solar energy collection and the aerodynamic performance of UAVs. Specifically, we focus on improving the UAVs' aerodynamic efficiency in flight, aligning it with energy optimization strategies to ensure sustained operation. The findings demonstrated significant improvements in the UAVs' range and weather resilience, thereby enhancing their utility for a variety of missions, including environmental monitoring and search and rescue operations. These advancements underscore the potential of integrating biomimicry and neural-network-based optimization in expanding the functional scope of solar UAVs.

Keywords: solar energy; aerodynamics; neural networks; evolutionary-based optimization; range optimization; UAVs; simulation

1. Introduction

Unmanned aerial vehicles (UAVs) have become increasingly important across various fields, from agriculture to defense [1]. These UAVs are used in a wide range of applications, such as monitoring crops, conducting surveillance, and delivering goods [2]. UAVs operate under a range of environmental conditions, from indoor operations to the challenging and unpredictable conditions of outdoor missions. The materials used in the construction of

UAVs determine their performance characteristics, such as weight, durability, and aerodynamics [3,4]. Common structural components include the airframe, wings, propulsion system, landing gear, and control surfaces. The airframe forms the backbone of the UAV, providing the necessary support for all other components. It is typically designed to be as light as possible while ensuring sufficient strength and rigidity [5]. Wings are designed to generate lift and are often equipped with ailerons, flaps, and other control surfaces to facilitate maneuverability. The propulsion system, which includes motors and propellers or turbines, is optimized for efficiency and thrust. Each part must be meticulously connected, and advanced modeling of the structure is required to ensure aerodynamic efficiency and structural integrity. Strong bolts and other fasteners must be used for durable connections, ensuring that the UAV can withstand operational stresses without component failure [6]. Advanced modeling techniques, such as computational fluid dynamics (CFD) and finite element analysis (FEA), are often employed to simulate and optimize the performance of UAVs under various conditions [7]. Despite structural considerations, the type of energy source also significantly impacts the range, endurance, and overall efficiency of UAVs [8]. As UAV usage expands, enhancing their flight paths for energy efficiency has become a significant engineering challenge [9–13]. This challenge is particularly significant for solar-powered UAVs that depend on a limited and variable supply of solar energy. Solar energy is not always available, and its availability can change based on the time of day and weather conditions. This reliance on solar power presents unique challenges, such as the need to maximize energy capture during sunlight hours and efficiently store this energy for continued operation [9,14–25].

1.1. Evolution and Integration of Solar Power

Initially conceptualized for military purposes, UAVs have evolved to become versatile tools in civilian and commercial domains [18]. Early UAV technology focused on military reconnaissance and target practice, but advancements in electronics, navigation, and materials science have enabled broader applications. The quest to extend the operational capabilities of UAVs led to the exploration of solar power as an additional energy source. Solar-powered UAVs emerged as a solution to the endurance limitations posed by onboard battery systems, marking a significant milestone with the integration of photovoltaic (PV) cells into UAV designs. High-altitude, long-endurance (HALE) UAVs, designed to operate at altitudes with intense and consistent solar radiation, have significantly extended mission durations [16–18,20,26–28].

1.2. Challenges in Solar Power Integration

Integrating solar power into UAVs presents several challenges. The efficiency of photovoltaic cells, the variability of solar energy, and the added weight of solar panels and energy storage systems impact UAV performance. For example, the efficiency of photovoltaic cells can vary significantly under different weather conditions. On cloudy days, these cells might not generate as much electricity as on sunny days. Additionally, batteries and other storage devices must be lightweight enough to allow the UAV to fly efficiently, but they also need to store enough energy to power the UAV for extended periods. To address these challenges, engineers have developed lightweight, high-efficiency photovoltaic cells and aerodynamically optimized designs to enhance energy efficiency [9,14,15,18,29,30].

1.3. Importance of Path Planning and Energy Management

Path planning is crucial for managing the energy consumption of UAVs. By optimizing their routes, UAVs can avoid areas where energy expenditure is high and take advantage of conditions favorable for solar energy capture. The integration of heuristic algorithms and machine learning techniques, particularly neural networks, offers promising avenues for improving flight path optimization. These technologies enable adaptive management of UAV flight paths in real time, enhancing their responsiveness to dynamic environmental conditions that impact solar energy availability. For instance, if a UAV

encounters unexpected cloud cover, it can adjust its flight path to move to an area with better sunlight [17–19,29,31–38].

The literature presents a range of strategies for path planning, from real-time adaptive algorithms to predetermined paths with minor in-flight adjustments. Real-time adaptive algorithms allow UAVs to continuously update their flight paths based on current conditions, while predetermined paths with minor adjustments provide a balance between flexibility and predictability. This diversity highlights the need for a balanced approach that harmonizes adaptability, energy efficiency, and operational reliability. An effective path planning strategy must be able to adapt to changing conditions without consuming too much energy in the process [9,14,15,17,19,39,40].

1.4. Heuristic Algorithms and Neural Networks

Heuristic algorithms play a significant role in refining neural networks for optimizing flight paths of solar-powered UAVs. Traditional methods may struggle with the dynamic nature of these paths, but heuristic approaches, such as Genetic Algorithms (GAs), Particle Swarm Optimization (PSO), or Simulated Annealing (SA), allow neural networks to adjust flight paths in real time. These heuristic methods are inspired by natural processes and are effective at finding solutions to complex problems. For example, Genetic Algorithms mimic the process of natural selection, while Particle Swarm Optimization is inspired by the social behavior of birds flocking together. This adaptability enhances UAVs' responsiveness to environmental changes affecting the solar energy availability. Heuristic algorithms are particularly advantageous because they efficiently navigate complex, multidimensional search spaces, finding optimal or near-optimal solutions with lower computational cost and time. This is crucial in scenarios with unpredictable environmental fluctuations, ensuring that solar-powered UAVs maintain optimal energy efficiency and operational reliability [17–19,41,42].

1.5. Proposed Method: Genetic Algorithm over Neural Network

The primary aim of this work is to explore the utility of heuristic algorithms in refining the neural networks that guide the flight paths of solar-powered UAVs. By combining these heuristic methods with realistic terrain simulations, we propose an efficient process for flight path optimization. Genetic Algorithms (GAs) mimic natural selection processes, generating potential solutions and iteratively refining them to find the most efficient paths. By combining GAs with neural networks, we aim to enhance real-time flight path adjustment and energy resource management. Realistic terrain simulations can mimic the conditions UAVs will face in actual missions, allowing for better testing and refinement of path planning strategies. This approach ensures optimal energy utilization, extending the operational duration and mission reliability [9,14,15,17,19,39,40].

This study contributes to UAV efficiency by offering a methodological advancement in flight path optimization for solar-powered UAVs. The integration of heuristic algorithms with realistic terrain simulations provides a novel perspective on maximizing energy capture and optimizing storage. By improving the energy efficiency, we can extend the operational duration of UAVs and increase their reliability in various applications, ultimately making them more effective tools for the tasks they are designed to perform. This research reflects a commitment to harmonizing technological progress with sustainability and operational excellence, promising significant advancements in solar-powered UAV technology [9,14,15,17–19,32,33,39,40,43].

1.6. Review of Existing Methods and Approaches

In recent years, various optimization techniques have been employed to enhance the efficiency of solar-powered UAVs, focusing on both energy management and aerodynamic performance. Traditional methods, such as Genetic Algorithms (GAs), Particle Swarm Optimization (PSO), and Simulated Annealing (SA), have been widely used to optimize UAV flight paths by dynamically adjusting to environmental conditions. These heuristic

approaches are effective at finding solutions to complex problems and have been extensively discussed in the literature [1,16].

For instance, Genetic Algorithms mimic the process of natural selection to iteratively refine potential solutions, making them suitable for real-time UAV path optimization in dynamic environments [8]. Similarly, Particle Swarm Optimization is inspired by the social behavior of birds flocking together and has been successfully applied to enhance the adaptive capabilities of UAVs, particularly in uncertain and fluctuating environmental conditions [15,20].

Despite the effectiveness of these methods, they often require significant computational resources and may struggle with real-time adaptation when environmental variables change rapidly [14,18]. Furthermore, conventional approaches tend to focus either on energy efficiency or aerodynamic optimization, rather than integrating both aspects holistically [19,21].

In contrast, this study leverages the Slime Mold Optimization (SMO) algorithm, a novel heuristic inspired by the foraging behavior of slime molds, to optimize the neural networks guiding UAV flight paths. The SMO algorithm not only balances exploration and exploitation effectively, but also adapts in real time to dynamic environmental changes, offering a more comprehensive solution for solar UAVs that must operate efficiently in varying conditions [36,44].

This approach represents advancement over traditional methods by integrating aerodynamic calculations and energy management strategies into a unified framework, thereby enhancing the operational duration and reliability of solar-powered UAVs [4,17,45].

2. Materials and Methods

The primary goal of this study was to enhance the control systems of an UAV by optimizing its neural network weights and biases through the use of Slime Mold Optimization (SMO). The UAV navigated a simulated terrain influenced by various factors, including solar angles, aerodynamic forces, and obstacles.

As illustrated in Figure 1, the process flow for optimizing the UAV control systems involved two main stages: neural network optimization and environmental interaction.

Figure 1a outlines the neural network optimization using SMO, while Figure 1b shows the environmental interaction, including terrain initialization, collision detection, and determining environmental difficulty.

2.1. Software and Libraries

All computational models and algorithms were implemented using Python3. The following libraries were used: NumPy (1.26.4) for numerical computations, TensorFlow (2.16.1) for neural network implementations, MealPy (3.0.1) for evolutionary-based optimizations, and Matplotlib (3.8.4) for data visualizations.

2.2. Neural Network Architecture

The study utilized a neural network architecture tailored for the optimization of the UAV control systems. The network was constructed to efficiently process inputs and generate precise control outputs, ensuring optimal UAV navigation.

Figure 1 illustrates the architecture of the neural network, detailing the flow from the input layer, through the hidden layers, and ending at the output layer. Each node in the input layer represents a specific input feature, while the nodes in the hidden and output layers represent the transformed features and final predictions, respectively. The connections indicate the flow of information, with weights and biases optimizing this flow, as described by the equation.

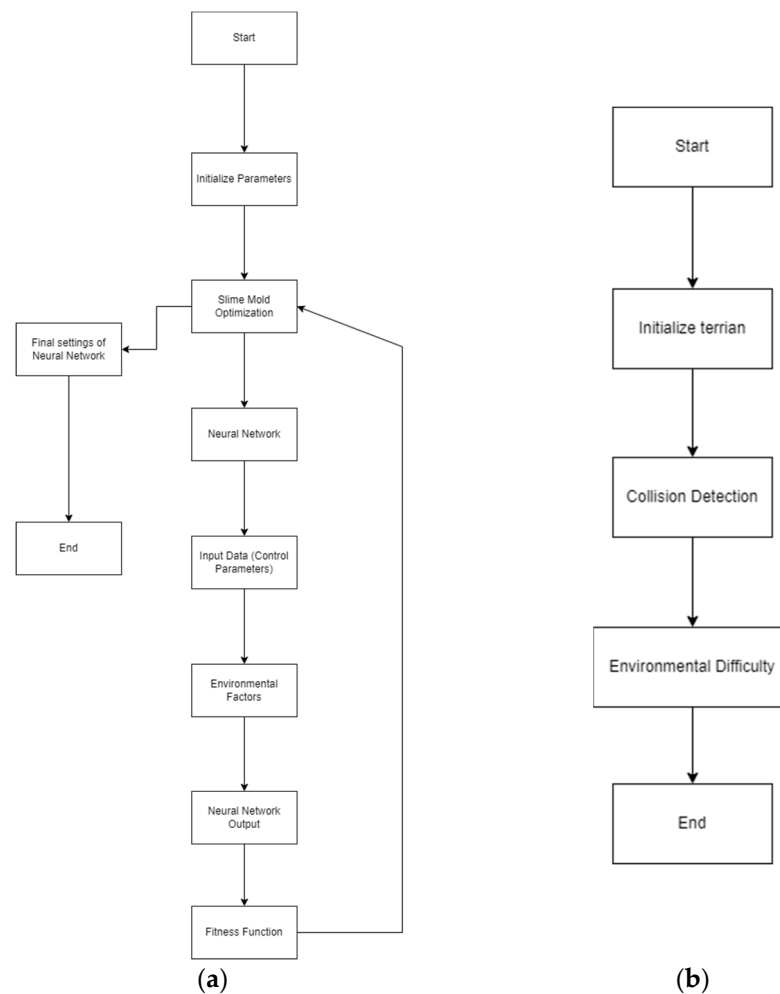


Figure 1. Process flow charts. (a) The neural network optimization process using Slime Mold Optimization (SMO). (b) The environmental interaction process for terrain navigation and obstacle avoidance.

The neural network is structured as a sequential model with three layers. Mathematically, each layer can be represented as:

$$h_i = \tanh(W_i \cdot x_i + b_i) \quad (1)$$

where h_i is the output after activation, \tanh is the hyperbolic tangent activation function, W_i denotes the weight matrix, x_i represents the input vector, and b_i is the bias term [32,44,46].

2.2.1. Activation Function

The neural network employed the hyperbolic tangent (\tanh) function as its activation mechanism. The \tanh function is advantageous, as it normalizes the output of neurons to a range between -1 and 1 . This feature is particularly beneficial for this network, as it ensures smoother gradients, effectively mitigating the risk of neuron saturation. Consequently, this facilitates a more efficient backpropagation process, crucial for the network's learning and adaptation capabilities [47].

2.2.2. Layer-Wise Breakdown

- (i) Input layer specifications—neuron count: The input layer comprises 22 neurons, each designed to process specific elements of the incoming data.

- (ii) Functional overview: The primary function of this input layer is to assimilate raw data, which, in the context of this study, encompasses a variety of environmental and operational parameters encountered by the UAV.
- (iii) Input parameters: The layer receives the following inputs, each representing critical aspects of the UAV's operational environment:
 1. Pitch: Reflecting the UAV's angular orientation along the lateral axis.
 2. Roll: Indicating the UAV's angular orientation along the longitudinal axis.
 3. Yaw: Representing the UAV's rotation around the vertical axis.
 4. Position (x, y, z): Spatial coordinates capturing the UAV's location in three-dimensional space.
 5. Span: Denoting the UAV's wingspan or a similar dimensional measurement relevant to its structure.
 6. Net force in y and z: Representing the total forces acting on the UAV in the vertical and lateral planes.
 7. Relative sunlight angle: Indicating the angle of sunlight relative to the UAV's orientation, crucial for solar-powered operations.
 8. Reduction of sunlight intensity due to clouds: Quantifying the decrease in solar energy availability due to cloud coverage.
 9. Time of day (azimuthal angle): Reflecting the sun's position, essential for understanding diurnal variations in environmental conditions [43].
 10. Current battery capacity: Indicating the UAV's available energy resources at any given moment.
 11. Maximum battery capacity: Denoting the UAV's total energy storage capability.
 12. Motor power and motor torque: Providing insights into the UAV's propulsion system's current operational status.
 13. Velocity (x, y, z): Capturing the UAV's speed across three dimensions.
 14. Closest object in x, y, z coordinates: Identifying the proximal objects in the UAV's immediate vicinity, critical for collision avoidance and navigational purposes.

These parameters collectively formed a comprehensive dataset, facilitating the neural network's initial processing phase and laying the foundation for complex, subsequent analytical processes.

2.2.3. Hidden Layers and Output Layer Architecture

The first hidden layer comprises 64 neurons, significantly enhancing the network's capability to discern complex patterns within the input data. This layer is pivotal in transforming the raw input into a more abstract representation, which facilitates deeper analysis in subsequent layers. The relatively high neuron count is instrumental in capturing intricate patterns and relationships within the data.

The second hidden layer consists of 32 neurons and further refines the data processing initiated by the first layer. Its primary role is to refine and consolidate the abstract representations formulated by the first hidden layer, ensuring that only the most critical patterns and features are preserved and passed on to the output layer. This enhances the neural network's efficiency and accuracy in processing data.

The output layer is configured with four neurons and serves as the final stage in the data-processing pipeline. It interprets the refined data from the hidden layers and generates the ultimate control commands for the UAV. The utilization of four neurons suggests that the network is designed to produce four distinct output parameters, each governing a specific aspect of UAV control.

2.2.4. Dynamic Weight Adjustment

During the optimization process, the weights of the neural network were adjusted as follows:

$$W_i^{new} = W_i \odot s \quad (2)$$

where new W_i new represents the new weights, W_i the original weights, s the solution vector from the optimization algorithm, and \odot denotes element-wise multiplication. Fine-tuning the network in such a manner enhanced the UAV's energy management and operational efficiency, directly contributing to more sustainable and extended missions under varying environmental conditions. This approach ensured that the UAV could adapt to different environmental scenarios, optimizing its performance and reducing energy consumption.

2.3. Slime Mold Algorithm (SMA)

The application of the Slime Mold Algorithm (SMA) targeted the optimization of the neural network's weights and biases to enhance the UAV's operational efficiency in diverse environmental conditions. The optimization process was designed over the neural network as in [44].

2.3.1. Optimization Goal

The principal objective was to optimize the UAV's operational parameters to achieve maximal efficiency, defined by a meticulously crafted fitness function. This function assessed the UAV's performance based on its energy management, adaptability to environmental conditions, and effective utilization of operational time.

2.3.2. Fitness Function

The UAV's fitness for operation was quantitatively assessed through the following fitness function:

$$\text{Fitness} = 19 \cdot (\text{end_battery}) - 2 \cdot (\text{start_time}) + \text{start_battery} + \text{num_clouds} + \text{num_obstacles} + \text{flight_time} \quad (3)$$

In this formula, *end_battery* represents the battery level at the end of the flight, *start_time* is the time at which the UAV starts its operation, *start_battery* denotes the battery level at the start of the flight, *num_clouds* indicates the number of clouds encountered during the flight, *num_obstacles* refers to the number of obstacles encountered during the flight, and *flight_time* is the total duration of the flight. This fitness function evaluates the UAV's performance by considering both its operational efficiency and the environmental conditions encountered. By optimizing these variables, the UAV can achieve better energy management and operational efficiency, ensuring more sustainable and extended missions under varying environmental conditions.

2.3.3. Conditions and Saturations

Battery status: Limited within the range [0, 1], where 1 signifies full battery capacity, and 0 indicates complete depletion.

Environmental constraints: These parameters are bounded by the physical and environmental characteristics of the operational domain, affecting navigation and sensor performance.

Operational time: This parameter incorporates diurnal variations, impacting mission planning and execution.

2.3.4. Cost Function

The cost function inherent within the fitness function aims to minimize adverse operational impacts, such as excessive energy consumption and reduced adaptability, while maximizing the UAV's operational efficiency. The optimization process thus involves a delicate balance, adjusting the UAV's operational parameters to optimize the overall fitness score.

2.3.5. Optimization Process

Initiated with a population size of 100, the SMA underwent 1000 iterations to ensure convergence to optimal solutions. A unique computational strategy was employed, where the weights in each row were multiplied by a common factor during each iteration to enhance the exploration efficiency within the solution space.

Through the SMA, the optimization of the neural network's weights and biases was methodically conducted, aligning with the defined fitness function. This strategic approach enabled the precise tuning of UAV operational parameters, underscoring the efficacy of SMA in complex system optimizations, particularly in enhancing UAV efficiency against a backdrop of variable environmental conditions and operational constraints.

2.4. Simulated Environment in Python

The simulated environment is pivotal for evaluating solar-powered UAVs' operational efficacy under varied conditions. This Python-based simulation incorporated azimuthal solar angles to mirror the sun's positional changes over time, which directly impacted the efficiency of the solar panels and, consequently, the energy availability for the UAVs. This simulation also introduced complex navigational scenarios with randomly distributed obstacles and cloud cover, which not only challenged flight path optimization but also realistically affected solar energy capture. Such a comprehensive setup is crucial for assessing the UAVs' adaptability to environmental dynamics and optimizing their flight paths for improved energy efficiency and reliability [21,43,48].

The environment factors were as follows:

1. **Grid size:** Defines the dimensions of the 3D environment.
2. **Number of obstacles:** Specifies the quantity of physical obstacles within the environment.
3. **Obstacle size:** The fixed side length of each cubic obstacle.
4. **Number of clouds:** Indicates the amount of cloud formations affecting sunlight.
5. **Cloud size:** The fixed side length of each cubic cloud.
6. **Sunlight intensity:** Varies based on time of day and cloud coverage, impacting solar energy calculations.
7. **Sun direction:** Determined by azimuth and altitude angles, influencing the solar panel efficiency.
8. **Temperature:** Changes with altitude, affecting atmospheric conditions.
9. **Pressure:** Atmospheric pressure, which decreases with altitude.
10. **Sunlight reduction factor:** Fraction of sunlight blocked by cloud coverage.
11. **Time of day:** Impacts the position of the sun and overall sunlight intensity.

2.5. Aerodynamics Calculation through the Vortex Lattice Method in Aerodynamics

The Vortex Lattice Method (VLM) is a semi-empirical approach used predominantly for estimating the aerodynamic properties of wings and aircraft bodies at subsonic speeds. Its fundamental principle lies in representing lifting surfaces as an assembly of bound vortices, offering a balance between computational efficiency and accuracy [35,46,49].

In VLM, discretization is essential for practical computation. In Figure 2, the discretization is drawn out. The aircraft's lifting surface is segmented into numerous discrete panels, typically rectangles or triangles. This segmentation facilitates a manageable yet detailed representation of the lifting surface. Each panel is endowed with a vortex that symbolizes the circulation over it, allowing for a granular analysis of the aerodynamic properties. The panels' center point is marked by the colored dot over the mesh.

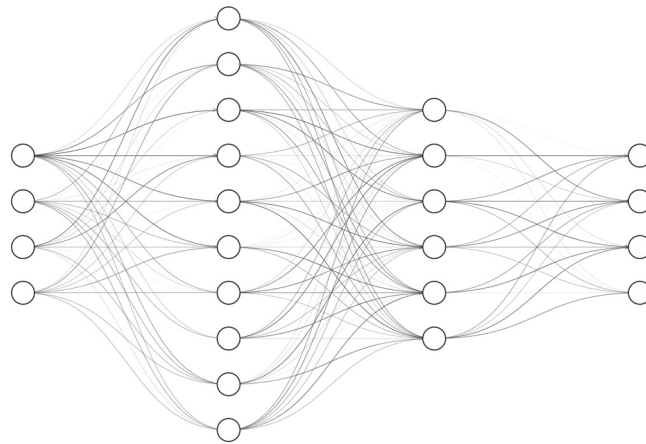


Figure 2. Neural network layout.

2.5.1. Horseshoe Vortex Model

The horseshoe vortex model is instrumental in VLM, simulating the aerodynamic effect of each panel on an aircraft. By representing the aerodynamic flow around the panel as a combination of a bound vortex and trailing vortices, this model allows for a detailed analysis of the lift generated by each panel. The strength of these vortices is directly tied to the circulation around the panel, providing a foundational parameter for calculating aerodynamic forces. This approach enables precise modeling of the lift forces acting on the aircraft.

2.5.2. Flow Tangency Condition

Integral to potential flow theory and VLM is the flow tangency condition. It posits that airflow remains tangent to the body's surface, preventing flow penetration. Mathematically, for a 2D panel j with vortex strength Γ_j , the condition is articulated as:

$$\sum_j \Gamma_j \cdot \text{Influence of vortex } j \text{ on panel } i = -V_{\infty,i} \cdot n_i \quad (4)$$

and \cdot is the symbol for the inner product.

This equation is fundamental in determining the vortex strengths, Γ_j , across all panels, where $V_{\infty,i}$ represents the free-stream velocity at panel i , and n_i is the unit normal to panel i [46].

After determination of the vortex strengths, the next step is computing the aerodynamic forces on each panel. The lift per unit span for a 2D panel is given by the formula:

$$L' = \rho V_{\infty} \Gamma \quad (5)$$

In this equation, ρ signifies air density, V_{∞} is the free-stream velocity, and Γ is the circulation around the panel [9,14,39,50].

The total lift is then the sum of the lift contributions from all the panels. Similarly, other aerodynamic quantities, such as drag, can also be estimated using additional considerations. In conclusion, VLM provides a computationally efficient way to compute aerodynamic properties of wings and aircraft bodies. While it does not capture viscous effects and is typically limited to subsonic flow, it is quite effective for preliminary design and analysis tasks.

Integrating the horseshoe vortex model and the flow tangency condition, VLM provides a robust framework for predicting the aerodynamic forces on an aircraft. The calculation of lift, through the determination of vortex strengths and the enforcement of flow tangency, showcases the method's capability in simulating complex aerodynamic interactions. Although VLM abstracts away some complexities, such as viscous effects, its computational efficiency and effectiveness in preliminary design and analysis remain

unparalleled. In our study, applying VLM to UAV aerodynamics allowed for a nuanced understanding of how design and environmental factors influence flight efficiency and responsiveness.

2.5.3. Discretization Calculations

To accurately model physical phenomena within the simulated environment, it is essential to compute the geometric properties of discrete elements.

Considering three points in 3D space, p_1 , p_2 , and p_3 , the area of the triangle they form is calculated as:

$$Area = \frac{1}{2} \| v_1 \times v_2 \| \quad (6)$$

where:

$$v_1 = p_2 - p_1 \quad (7)$$

$$v_2 = p_3 - p_1 \quad (8)$$

and the symbol \times means the outer (vector) product.

For a quadrilateral defined by four points, the total area is the sum of the areas of two triangles formed by splitting the quadrilateral:

$$Total_Area = Area_{triangle1} + Area_{triangle2} \quad (9)$$

The normal vector to the wing (or UAV surface) is calculated using the cross-product of vectors formed by its diagonal points:

$$UAV_{normal} = \frac{(points[2] - points[0]) \times (points[3] - points[1])}{(points[2] - points[0]) \times (points[3] - points[1])} \quad (10)$$

For a rotation defined by angles α , β , and γ , being pitch, roll, and yaw, respectively, the rotation matrix, D , is:

$$D = \begin{bmatrix} \cos(\beta)\cos(\gamma) & \sin(\alpha)\sin(\beta)\cos(\gamma) - \cos(\alpha)\sin(\gamma) & \cos(\alpha)\sin(\beta)\cos(\gamma) + \sin(\alpha)\sin(\gamma) \\ \cos(\beta)\sin(\gamma) & \sin(\alpha)\sin(\beta)\sin(\gamma) + \cos(\alpha)\cos(\gamma) & \cos(\alpha)\sin(\beta)\sin(\gamma) - \sin(\alpha)\cos(\gamma) \\ -\sin(\beta) & \sin(\alpha)\cos(\beta) & \cos(\alpha)\cos(\beta) \end{bmatrix} \quad (11)$$

For mirroring points along a given axis, the reflection matrix is calculated as:

$$Reflection_Matrix = I - 2 \cdot axis \times axis^T \quad (12)$$

where I is the identity matrix and $axis$ is the unit vector along which reflection is performed.

2.5.4. VLM Calculations

The Vortex Lattice Method (VLM) is a computational technique used to estimate the aerodynamic forces and velocity fields around lifting surfaces, such as the wings of an aircraft or, in our case, a UAV. These calculations are crucial for predicting aerodynamic performance and informing the design and control system optimization.

The velocity induced at a point p by a trailing vortex line starting at r and ending at r_2 is given by:

$$V_{trail} = \frac{\alpha + 1}{4\pi h} \quad (13)$$

where:

$$h = \frac{\| (p - r) \times (p - r_2) \|}{\| r_2 - r \|} \quad (14)$$

and:

$$\alpha = -\frac{(p - r) \cdot (r_2 - r)}{\| r_2 - r \|} \quad (15)$$

The velocity induced at a point p by a bound vortex line between r and s is:

$$V_{bound} = \frac{\alpha + \beta}{4\pi(-h)} \quad (16)$$

where:

$$h = -\frac{\|(p-r) \times (p-s)\|}{\|s-r\|} \quad (17)$$

and:

$$\beta = \frac{(s-r) \cdot (p-r)}{\|p-r\|} \quad (18)$$

and:

$$\alpha = -\frac{(s-r) \cdot (p-s)}{\|p-s\|} \quad (19)$$

The AIC matrix is computed using the velocities induced by the trailing and bound vortex lines. For each panel i and j , the AIC matrix element, $AIC[i][j]$, is given by:

$$AIC[i][j] = b_v + l_v - r_v \quad (20)$$

where b_v , l_v , and r_v are the velocities due to bound, left trailing, and right trailing vortex lines, respectively, computed using the above formulas.

2.5.5. Solving the VLM System

The VLM system is solved by calculating the circulation strength (γ) for each panel. This is achieved by solving the linear system:

$$AIC \cdot \gamma = V_{inf} \quad (21)$$

where V_{inf} is the free-stream velocity vector, and γ is the circulation strength vector.

2.5.6. Lift and Drag Calculation

The lift and drag are then computed using:

$$\text{Lift} = \sum \rho V_{mag} \gamma_i \text{span}_i \quad (22)$$

$$\text{Drag} = \sum \rho \gamma_i \text{span}_i \text{VID}_i \quad (23)$$

where ρ is the air density, V_{mag} is the magnitude of the free-stream velocity, γ_i is the circulation strength of the i -th panel, span_i is the span of the i -th panel, and VID_i is the down wash velocity induced at the i -th panel.

2.6. Dynamic Environment

A dynamic element was introduced through the application of VLM at every simulation time step. This continuous recalibration of aerodynamic forces allowed the UAV to adjust promptly to changing conditions and maneuvers, showcasing the method's adaptability in dynamic scenarios. In this dynamic environment, we had to consider performing calculations of the environment at given moments, and they are shown below.

2.6.1. Calculation of Pressure

The pressure at a given altitude, H (in meters), is calculated using the barometric formula:

$$P = P_0 \left(1 - \frac{L \cdot H}{T_0}\right)^{\frac{g \cdot M}{R \cdot T}} \quad (24)$$

where P_0 is the pressure at sea level, L is the lapse rate, T_0 is the standard temperature at sea level, g is the acceleration due to gravity, M is the molar mass of dry air, and R is the ideal gas constant.

2.6.2. Calculation of Density

The density of the air at a given pressure and temperature is calculated using the ideal gas law:

$$\rho = \frac{P}{0.2869 \cdot \text{temperature}} \quad (25)$$

2.6.3. Relative Sunlight Angle

The relative sunlight angle is crucial for accurately calculating the solar power output of the UAV. It determines the efficiency of solar energy capture by the UAV's panels, as the power output is directly influenced by how directly sunlight strikes the panels. A more perpendicular angle (closer to 0 degrees) between sunlight and the UAV surface maximizes energy absorption, while an acute or obtuse angle reduces it [51]. This calculation, incorporating the angle of incidence and later potential cloud cover reduction, allows for precise estimation of available power, critical for energy management and flight path optimization in solar-powered UAVs [13]. The relative angle between the sunlight direction and a UAV normal vector is calculated using the dot product:

$$\text{angle} = \arccos \left(\frac{\text{sun_direction} \cdot \text{uav_normal}}{\| \text{sun_direction} \| \cdot \| \text{uav_normal} \|} \right) \quad (26)$$

2.6.4. Calculation of Solar Output

The solar power output, considering the angle of incidence and cloud cover, is given by:

$$\text{output} = \text{wing_area} \cdot 1000 \cdot \cos(\text{angle}) \cdot \text{cloud_sunlight_reduction} \quad (27)$$

2.7. Simulated Battery Cycles

Simulating battery cycles mimics the charging and discharging patterns a battery undergoes throughout its lifecycle. This process is critical for understanding energy management within the UAV system, especially in relation to battery sizing and its compatibility with the propulsion system. The developed model incorporates key factors, such as flight duration, energy consumption rates, and charge/discharge frequencies, to emulate real-world UAV operations.

The simulation not only predicts potential capacity loss, changes in internal resistance, and overall battery degradation, but also assesses the suitability of the battery configuration for the UAV's propulsion demands. Specifically, the battery's capacity and voltage are carefully calculated to ensure that they are sufficient to power the motor under various operating conditions. The equations used in the model include:

$$\text{minvoltage} = 3.25 \cdot \text{seriescells} \quad (28)$$

$$\text{maxvoltage} = 4.2 \cdot \text{seriescells} \quad (29)$$

$$\text{maxcapacity} = \text{cellcapacity} \cdot \text{parallelcells} \quad (30)$$

By analyzing these simulated cycles, we can make informed decisions about the optimal battery size and capacity required for the UAV's propulsion system. This analysis could also be further improved on via integration of hybrid storage systems, such as combining batteries with supercapacitors, to enhance energy management. A hybrid storage system could provide the UAV with the capability to handle short bursts of high-power demand while maintaining overall energy efficiency during longer missions.

2.7.1. Voltage Calculation Based on Capacity

The voltage based on the current capacity is calculated using a polynomial equation:

$$\text{Voltage} = -3 \cdot 10^{-10} \cdot bp^5 + 1 \times 10^{-7} \cdot bp^4 - 1 \cdot 10^{-5} \cdot bp^4 + 8 \cdot 10^{-4} \cdot bp^3 - 0.027 \cdot bp^2 + 0.4345 \cdot bp + \text{min_voltage} \quad (31)$$

where bp is the battery percentage, calculated as $100 \cdot \text{capacity} / \text{max battery capacity}$.

2.7.2. Cycle Calculation

The number of cycles is calculated based on the change in voltage:

$$\text{cycles} = \frac{1}{2^{10 \cdot (\text{max_voltage_end_v})}} - \frac{1}{2^{10 \cdot (\text{max_voltage_start_v})}} \quad (32)$$

2.8. Battery Life and Thrust-to-Power Analysis

Battery life is pivotal for UAVs, especially when considering energy management for long-duration missions or remote operations. The thrust-to-power ratio, which determines the efficiency of the motor-propeller combination, plays a key role in this context. By analyzing this ratio, we can determine the most energy-efficient configurations that align with the UAV's power availability and battery capacity.

In our analysis, simulated battery cycles were used to evaluate battery health over time, taking into account the impact of energy management strategies, such as optimal charging, propulsion needs, and the potential for integrating hybrid storage systems. The findings from this analysis inform decisions on mission length, payload capabilities, and energy-intensive operations, ensuring that the UAV operates within its energy constraints while maximizing performance [9,12,45,52].

2.9. Analysis with Different Configurations

Two distinct motor types and two propeller configurations were analyzed, with a total of four combinations studied to optimize energy utilization. The analysis involved generating thrust-to-power plots for each combination to evaluate the efficiency of each motor-propeller pair.

The data collected from this analysis were crucial not only for identifying the optimal configuration but also for understanding the energy management trade-offs inherent in each setup. For instance, one motor-propeller combination might offer more thrust at a higher power cost, making it suitable for short, high-intensity missions, while another might provide lower thrust but with greater energy efficiency, making it ideal for longer, low-power missions. Integrating insights from these analyses with energy management strategies, such as the potential use of hybrid storage systems, allowed us to optimize the UAV's operational capabilities and extend its mission endurance.

2.10. Dynamic Environment in the Code

In the simulation framework, a conceptual buffer mechanism is proposed, based on the UAV's hypothetical current position, to enhance the loading time of the environment. In simulation contexts, the buffer is a preloaded segment of data or precomputed results that encompass a dynamic point of interest. This approach avoids the need for continuous computation or loading of data for the entire simulated environment. Instead, the simulation dynamically concentrates on a localized area around the current focal point, which, in practice, would be the UAV's position.

The benefits of such a buffer system, if implemented, would include that the simulation would manage a smaller, localized dataset, allowing for rapid loading or computation of pertinent data, resulting in faster response times. By focusing on a buffered region rather than an extensive landscape, computational power is allocated more efficiently, processing only the immediate vicinity of the UAV's hypothetical position.

The buffer system is designed to adapt as the focal point shifts, such as if a UAV were to traverse through the environment. The buffer is not static—it would be programmed to predict the UAV's movement and start processing data for the upcoming region in advance, while phasing out data no longer pertinent to the UAV's trajectory.

Integration with UAV systems is a key aspect of the buffer's operational concept. Navigation and sensor data, such as the UAV's projected position and path, would inform the buffer's updates, keeping relevant data ready for use.

This buffering strategy is particularly useful for handling environments with varying complexity. As the simulated UAV approaches areas with more intricate details, the buffer's algorithms would prioritize the loading of these specifics, ensuring that the simulation remains as efficient as possible.

2.11. Propulsion and Mission Phases

Regarding the propulsion system's performance and its relation to different mission phases, it is important to note that the proposed layout was designed to handle the specific requirements due to the UAV's spawn point being mid-air, and the primary focus during the initial phase of the simulation was on cruising rather than takeoff or landing. This configuration assumes the UAV is already at an altitude, thus bypassing the complexities of ground-based takeoff and focusing on efficient navigation and energy management once airborne.

The UAV is required to navigate efficiently once it has reached a sufficient altitude, where the propulsion system is optimized for sustaining long-duration flights at cruising altitudes. The buffer mechanism and the dynamic environment were thus calibrated to respond to the UAV's movement in this specific context, ensuring that data processing remained relevant to the cruising phase, where energy efficiency and real-time adaptability are paramount.

This approach aligned the simulation more closely with realistic mission profiles that emphasized extended operation at altitude, where the UAV's primary tasks, such as surveillance or communication relay, take place. Future work could expand on this framework by simulating additional mission phases, such as takeoff and landing, to provide a more comprehensive evaluation of the propulsion system's performance across all mission profiles.

3. Results

3.1. Iterative Analysis

The first iteration involved significant time investment, primarily due to the initial exploration phase and the complexities in defining the neural network's end goals. This foundational phase was critical in laying the groundwork for effective optimization in subsequent iterations.

The observed decrease in computational time for the simulation is illustrated in Figure 3. The system had a 12th Gen Intel Core i7-12700H processor, which provides a robust platform for the intensive calculations required in the optimization process. Initially, the simulations' first iteration took between 2 and 3 h to complete. However, subsequent iteration runs showed a significant reduction in time, with optimization processes taking 1 h or less.

By the fifth run, exploration constituted about 50% of the algorithm's process, indicating a well-balanced approach in probing new strategies for the neural network's learning. This balance between exploration and exploitation is graphically represented in Figure 4a, and Figure 4b shows the runtime.

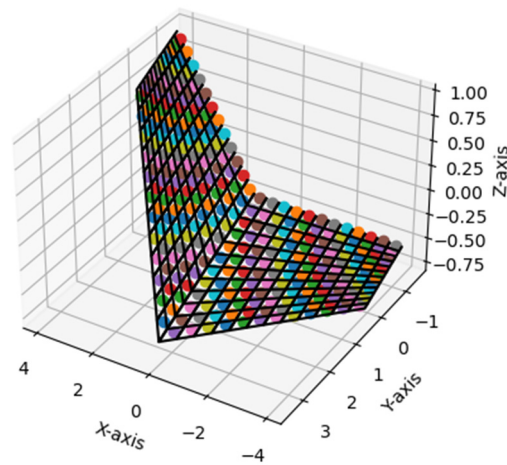
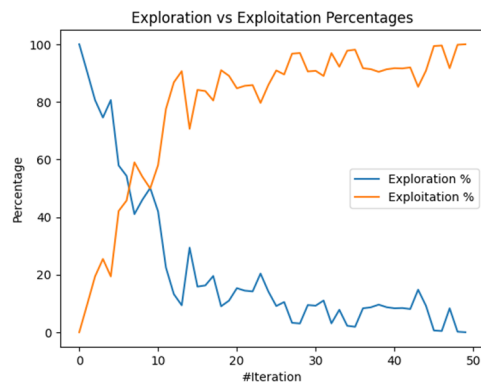
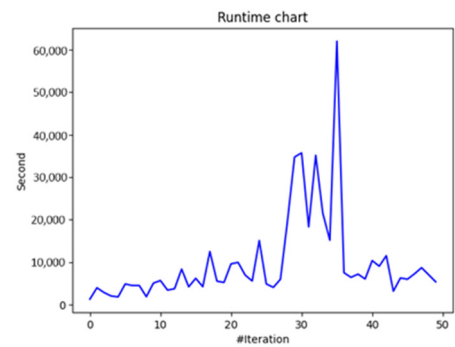


Figure 3. VLM discretization scheme (x, y, z in meters).



(a)



(b)

Figure 4. Optimization results: (a) exploration vs. exploitation and (b) runtime.

3.2. Time Analysis

The temporal efficiency of the Slime Mold Algorithm in optimizing the UAV’s neural network was a big aspect of this study. The initial iteration was the most time-consuming due to the intricate process of defining and tuning the neural network’s parameters, which was critical for establishing a robust foundation for the algorithm’s subsequent operations.

A consistent decrease in processing time was observed across iterations, highlighting the neural network’s improving computational efficiency and accelerated learning rate. This trend reflects the algorithm’s capacity to adapt and optimize more effectively with each iteration.

The balanced approach between exploration and exploitation within the algorithm underscores its adaptability to the neural network’s evolving learning needs. The initial time investment, though substantial, was justified by the efficiency gains in subsequent iterations.

The Slime Mold Algorithm showed promise in optimizing the neural network for a solar-powered UAV. Its ability to balance exploration and exploitation led to enhanced performance over successive iterations, with the initial investment in time proving crucial to the optimization process.

Future studies should consider expanding the scope by increasing the number of iterations and incorporating a wider range of performance metrics. Additionally, applying the Slime Mold Algorithm to different types of neural networks or UAV applications could provide further insights into its adaptability and efficiency in various contexts.

This study contributes to the field of AI-powered control systems for UAVs, particularly those relying on solar energy. By utilizing the Slime Mold Algorithm for neural

network optimization, this study offered an alternative approach to traditional methods. The results demonstrated the potential of such algorithms in fine-tuning the weights and biases of neural networks, thereby enhancing the functionality and autonomy of solar-powered UAVs. The successful application of this algorithm in developing an AI-driven solar UAV control system supports its potential effectiveness in similar contexts.

The success of the Slime Mold Algorithm in this study suggests new avenues for integrating hyper-heuristic algorithms into UAV control systems, especially in challenging environments. As current systems approach performance limits, exploring multiple optimization algorithms could further improve UAVs' efficiency and decision-making capabilities. This direction is promising for the future of UAV technology, particularly in scenarios requiring autonomous operation in complex environments.

4. Conclusions

This study marks as an effort in the application of the Slime Mold Algorithm for optimizing neural networks in solar-powered UAV control systems. The findings highlighted the complexities and challenges of integrating AI and optimization algorithms into advancing UAV technologies. Although the Slime Mold Algorithm demonstrated potential in achieving rapid convergence in the solution space and a balance between exploration and exploitation, its overall effectiveness in enhancing UAV performance encountered certain limitations.

The integration of the Vortex Lattice Method (VLM) into our UAV simulation framework was a crucial aspect of our study. VLM provided a balance between computational efficiency and accuracy, which was valuable for our simulation needs.

The advancement in our research also involved incorporating solar panel efficiency calculations as a function of the azimuthal solar angle. This consideration allowed for optimized energy capture, which is essential for the prolonged operation of solar-powered UAVs. The ability to adapt flight paths and maneuvers based on solar energy availability was a key factor in enhancing the UAV's energy efficiency.

Furthermore, the UAV's control system, designed to navigate through simulated terrain, leveraged outputs from the optimized neural network. This integration translated into adjustments in thrust and changes in the UAV's pitch, roll, and yaw, enabling efficient maneuverability and responsiveness to environmental variables.

Insights into solar panel efficiency during flight for the simulation were also taken into account for the UAV's operational decisions. This adaptability, informed by continuous updates on solar efficiency, equipped the neural network to make informed control decisions. It could prioritize energy conservation during periods of low efficiency or allocate more power for energy-intensive tasks when efficiency was high. The neural network's capability to learn and adapt based on historical data further enhanced the UAV's operational efficiency.

In conclusion, the synergy of aerodynamics, control logic, and energy optimization, through the integration of VLM, a sophisticated control system, and adaptive solar energy management, underscores the potential of integrating multiple technologies for enhanced UAV performance in varied operational scenarios. Incorporating the efficiency of solar panels as a function of the azimuthal solar angle into the UAV's neural network control system enabled dynamic, adaptive, and energy-efficient decision-making. This holistic approach ensured that the UAV not only responded to immediate environmental and operational challenges but also learned from them for future operations.

While the study demonstrated advancements in utilizing the Slime Mold Algorithm for neural network optimization in solar-powered UAVs, it also brought to light certain limitations that warrant further exploration. One notable area was the reliance on a restricted set of inputs, which presented challenges for integrating real-time data during actual flight operations. Additionally, the integration of technologies—such as the Vortex Lattice Method with solar panel efficiency calculations into the UAV's control systems—merits further refinement to achieve seamless operation. These challenges, coupled with

the complexities of real-time AI integration for autonomous UAV operation in dynamic environments, highlight the necessity of continued research. By addressing these aspects, future studies can expand upon the work laid out here, exploring a broader range of technologies and strategies to enhance the adaptability and efficiency of UAV systems, thus fully realizing the transformative potential of AI in autonomous UAV technology.

Author Contributions: Conceptualization, G.H.; methodology, G.H. and F.S.S.; software, G.H.; validation, D.M., A.H., M.N. and G.H.; formal analysis, D.M., A.H., G.H., M.N. and W.G.; investigation, G.H.; data curation, G.H.; writing—original draft preparation, G.H. and G.S.; writing—review and editing, M.T.H.S., A.H., D.M., F.S.S., G.S., M.N., I.M. and W.G.; visualization, G.H.; supervision, M.T.H.S., A.H., D.M. and W.G.; project administration, F.S.S. and M.N.; funding acquisition, M.T.H.S., M.N., D.M., A.H. and W.G. All authors have read and agreed to the published version of the manuscript.

Funding: The authors are grateful for the financial support given by The Ministry of Higher Education Malaysia (MOHE) under the Higher Institution Centre of Excellence (HICOE2.0/5210004) at the Institute of Tropical Forestry and Forest Products.

Institutional Review Board Statement: Not applicable.

Informed Consent Statement: Not applicable.

Data Availability Statement: The data that support the findings of this study are available from the author upon reasonable request.

Acknowledgments: The authors would like to thank the Department of Aerospace Engineering, Faculty of Engineering, Universiti Putra Malaysia, and Laboratory of Biocomposite Technology, Institute of Tropical Forestry and Forest Product (INTROP), Universiti Putra Malaysia, for the close collaboration in this research.

Conflicts of Interest: The authors declare no conflicts of interest.

References

- Laghari, A.; Jumani, A.K.; Laghari, R.A.; Nawaz, H. Unmanned aerial vehicles: A review. *Cogn. Robot.* **2023**, *3*, 8–22. [[CrossRef](#)]
- Molina, A.A.; Huang, Y.; Jiang, Y. A Review of Unmanned Aerial Vehicle Applications in Construction Management: 2016–2021. *Standards* **2023**, *3*, 95–109. [[CrossRef](#)]
- Anand, S.; Mishra, A.K. High-Performance Materials used for UAV Manufacturing: Classified Review. *Int. J. All Res. Educ. Sci. Methods (IJARESM)* **2022**, *10*, 2811–2819. ISSN 2455-6211.
- Pugi, L.; Berzi, L.; Favilli, S.; Franchi, L.; Mattei, G.; Fiorenzani, R.; Casazza, A. An Innovative Uav with Vtol Capabilities. *Int. J. Mech. Control* **2023**, *24*, 135–148. [[CrossRef](#)]
- Kopania, J.M.; Zakrzewicz, W.; Kubiak, P.; Mrowicki, A.; Głogowski, M.; Gralewski, J.; Bogusławski, G.; Wójciak, K.; Gaj, P. The Properties of Materials and Structures of Fluted PVC Panels for the Transmission of Airborne Sound. *Appl. Sci.* **2022**, *12*, 5732. [[CrossRef](#)]
- Grzejda, R.; Parus, A.; Kwiatkowski, K. Experimental studies of an asymmetric multi-bolted connection under monotonic loads. *Materials* **2021**, *14*, 2353. [[CrossRef](#)]
- Sidun, P.; Łukaszewicz, A. Verification of ram-press pipe bending process using elasto-plastic FEM model. *Acta Mech. Autom.* **2017**, *11*, 47–52. [[CrossRef](#)]
- Saravanakumar, Y.N.; Sultan, M.T.H.; Shahar, F.S.; Giernacki, W.; Łukaszewicz, A.; Nowakowski, M.; Holovatyy, A.; Stępień, S. Power Sources for Unmanned Aerial Vehicles: A State-of-the Art. *Appl. Sci.* **2023**, *13*, 11932. [[CrossRef](#)]
- Wirth, L.; Oettershagen, P.; Ambühl, J.; Siegwart, R. Meteorological Path Planning Using Dynamic Programming for a Solar-Powered UAV. In Proceedings of the Aerospace Conference, Big Sky, MT, USA, 7–14 March 2015; IEEE: Piscataway, NJ, USA, 2015.
- Grodzki, W.; Łukaszewicz, A. Design and manufacture of unmanned aerial vehicles (UAV) wing structure using composite materials. *Mater. Werkst.* **2015**, *46*, 269–278. [[CrossRef](#)]
- Łukaszewicz, A.; Szafran, K.; Józwiak, J. CAx techniques used in UAV design process. In Proceedings of the IEEE 7th International Workshop on Metrology for AeroSpace (MetroAeroSpace), Pisa, Italy, 22–24 June 2020; pp. 95–98. [[CrossRef](#)]
- Šančić, T.; Brčić, M.; Kotarski, D.; Łukaszewicz, A. Experimental Characterization of Composite-Printed Materials for the Production of Multicopter UAV Airframe Parts. *Materials* **2023**, *16*, 5060. [[CrossRef](#)]
- Chandran, N.K.; Sultan, M.T.H.; Łukaszewicz, A.; Shahar, F.S.; Holovatyy, A.; Giernacki, W. Review on Type of Sensors and Detection Method of Anti-Collision System of Unmanned Aerial Vehicle. *Sensors* **2023**, *23*, 6810. [[CrossRef](#)] [[PubMed](#)]

14. Padilla, G.E.G.; Kim, K.J.; Park, S.H.; Yu, K.H. Flight Path Planning of Solar-Powered UAV for Sustainable Communication Relay. *IEEE Robot. Autom. Lett.* **2020**, *5*, 6772–6779. [[CrossRef](#)]
15. Wu, J.; Wang, H.; Li, N.; Yao, P.; Huang, Y.; Yang, H. Path planning for solar-powered UAV in urban environment. *Neurocomputing* **2018**, *275*, 2055–2065. [[CrossRef](#)]
16. Aggarwal, S.; Kumar, N. Path planning techniques for unmanned aerial vehicles: A review, solutions, and challenges. *Comput. Commun.* **2020**, *149*, 270–299. [[CrossRef](#)]
17. Huang, Y.; Wang, H.; Yao, P. Energy-optimal path planning for Solar-powered UAV with tracking moving ground target. *Aerosp. Sci. Technol.* **2016**, *53*, 241–251. [[CrossRef](#)]
18. Oettershagen, P.; Förster, J.; Wirth, L.; Hitz, G.; Siegwart, R.; Ambühl, J. Meteorology-aware multi-goal path planning for large-scale inspection missions with solar-powered aircraft. *J. Aerosp. Inf. Syst.* **2019**, *16*, 390–408. [[CrossRef](#)]
19. Lee, J.S.; Yu, K.H. Optimal Path Planning of Solar-Powered UAV Using Gravitational Potential Energy. *IEEE Trans. Aerosp. Electron. Syst.* **2017**, *53*, 1442–1451. [[CrossRef](#)]
20. Wang, X.; Yang, Y.; Wang, D.; Zhang, Z. Mission-oriented cooperative 3D path planning for modular solar-powered aircraft with energy optimization. *Chin. J. Aeronaut.* **2022**, *35*, 98–109. [[CrossRef](#)]
21. Klesh, A.T.; Kabamba, P.T. Solar-powered aircraft: Energy-optimal path planning and perpetual endurance. *J. Guid. Control Dyn.* **2009**, *32*, 1320–1329. [[CrossRef](#)]
22. Vasisht, S.; Mesbahi, M. Trajectory design and coverage control for solar-powered UAVs. In Proceedings of the AIAA Guidance, Navigation, and Control Conference 2015, MGNC 2015, Kissimmee, FL, USA, 5–9 January 2015. [[CrossRef](#)]
23. Huang, Y.; Wang, H.; Chen, J.; Liu, R.; Su, G.; Du, P. Energy-optimal path planning for solar-powered UAVs monitoring stationary target. In Proceedings of the 4th ACM SIGSPATIAL International Workshop on Safety and Resilience, EM-GIS 2018, Seattle WA, USA, 6 November 2018. [[CrossRef](#)]
24. Du, N.; Zhang, Z.; Chen, J.; Liu, X.; Zhang, K.; Ma, B. A Coverage Path Planning Method Based on Multiple Solar Powered Unmanned Aerial Vehicles. In Proceedings of the IEEE International Conference on Unmanned Systems and Artificial Intelligence (ICUSAI), Xi'an, China, 22–24 November 2019. [[CrossRef](#)]
25. Hosseini, S.; Mesbahi, M. Energy-aware aerial surveillance for a long-endurance solar-powered unmanned aerial vehicle. *J. Guid. Control Dyn.* **2016**, *39*, 1980–1993. [[CrossRef](#)]
26. Qu, C.; Gai, W.; Zhong, M.; Zhang, J. A novel reinforcement learning based grey wolf optimizer algorithm for UAVs path planning. *Appl. Soft Comput. J.* **2020**, *89*, 106099. [[CrossRef](#)]
27. Zephyr-UAV-Airbus. Available online: <https://www.airbus.com/en/products-services/defence/uas/uas-solutions/zephyr> (accessed on 4 July 2024).
28. Mishra, A.; Pal, S.; Singh, P. Recent Trends in Long Endurance Solar Powered UAVs: A Review Article in. *Int. J. Adv. Sci. Technol.* **2020**, *29*, 6009–6018. Available online: <https://www.researchgate.net/publication/342153671> (accessed on 3 July 2024).
29. Gao, X.Z.; Hou, Z.X.; Guo, Z.; Liu, J.X.; Chen, X.Q. Energy management strategy for solar-powered high-altitude long-endurance aircraft. *Energy Convers. Manag.* **2013**, *70*, 20–30. [[CrossRef](#)]
30. Li, Z.; Liu, F.; Yang, W.; Peng, S.; Zhou, J. A Survey of Convolutional Neural Networks: Analysis, Applications, and Prospects. *IEEE Trans. Neural Netw. Learn. Syst.* **2022**, *33*, 6999–7019. [[CrossRef](#)]
31. Smith, H.; Rajendran, P. Review of the Elementary Aspect of Small Solar-powered Electric Unmanned Aerial Vehicles. *Aust. J. Basic Appl. Sci.* **2014**, *8*, 252–259.
32. Yao, P.; Wang, H.; Su, Z. Real-time path planning of unmanned aerial vehicle for target tracking and obstacle avoidance in complex dynamic environment. *Aerosp. Sci. Technol.* **2015**, *47*, 269–279. [[CrossRef](#)]
33. Yao, P.; Wang, H.; Su, Z. UAV feasible path planning based on disturbed fluid and trajectory propagation. *Chin. J. Aeronaut.* **2015**, *28*, 1163–1177. [[CrossRef](#)]
34. Yao, P.; Wang, H.; Su, Z. Cooperative path planning with applications to target tracking and obstacle avoidance for multi-UAVs. *Aerosp. Sci. Technol.* **2016**, *54*, 10–22. [[CrossRef](#)]
35. Voß, A. An Implementation of the Vortex Lattice and the Doublet Lattice Method Version 1.05. Available online: <https://elib.dlr.de/136536/> (accessed on 4 July 2024).
36. Chen, H.; Li, C.; Mafarja, M.; Heidari, A.A.; Chen, Y.; Cai, Z. Slime mould algorithm: A comprehensive review of recent variants and applications. *Int. J. Syst. Sci.* **2023**, *54*, 204–235. [[CrossRef](#)]
37. Slowik, A.; Kwasnicka, H. Evolutionary algorithms and their applications to engineering problems. *Neural Comput. Appl.* **2020**, *32*, 12363–12379. [[CrossRef](#)]
38. Kandikjan, T.; Djokikj, J.; Mircheski, I.; Angeleska, E. Integrating parametric design and additive manufacturing knowledge in Industrial design education. *Mater. Today Proc.* **2022**, *70*, 687–693. [[CrossRef](#)]
39. Klesh, A.T.; Kabamba, P.T. Energy-Optimal Path Planning for Solar-Powered Aircraft in Level Flight. In Proceedings of the Navigation and Control Conference and Exhibit, Hilton Head, SC, USA, 20 August–23 August 2007. [[CrossRef](#)]
40. Dai, R.; Lee, U.; Hosseini, S.; Mesbahi, M. Optimal pathplanningfor solar-powered UAVs based on unitquaternions. In Proceedings of the IEEE 51st IEEE Conference on Decision and Control (CDC), Maui, HI, USA, 10–13 December 2012; pp. 3104–3109. [[CrossRef](#)]
41. Isaac Abiodun, O.; Jantan, A.; Esther Omolara, A.; Victoria Dada, K.; AbdElatif Mohamed, N.; Arshad, H. State-of-the-art in artificial neural network applications: A survey. *Heliyon* **2018**, *4*, e00938. [[CrossRef](#)] [[PubMed](#)]

42. Mateja, K.; Skarka, W.; Peciak, M.; Niestrój, R.; Gude, M. Energy Autonomy Simulation Model of Solar Powered UAV. *Energies* **2023**, *16*, 479. [[CrossRef](#)]
43. Kim, S.H.; Padilla, G.E.G.; Kim, K.J.; Yu, K.H. Flight Path Planning for a Solar Powered UAV in Wind Fields Using Direct Collocation. *IEEE Trans. Aerosp. Electron. Syst.* **2020**, *56*, 1094–1105. [[CrossRef](#)]
44. Li, S.; Chen, H.; Wang, M.; Heidari, A.A.; Mirjalili, S. Slime mould algorithm: A new method for stochastic optimization. *Future Gener. Comput. Syst.* **2020**, *111*, 300–323. [[CrossRef](#)]
45. Huang, Y.; Chen, J.; Wang, H.; Su, G. A method of 3D path planning for solar-powered UAV with fixed target and solar tracking. *Aerosp. Sci. Technol.* **2019**, *92*, 831–838. [[CrossRef](#)]
46. Voß, A. Comparison between VLM and CFD Maneuver Loads Calculation at the Example of a Flying Wing Configuration. *ASD J.* **2019**, *7*, 19–37. [[CrossRef](#)]
47. Sharma, S.; Sharma, S.; Athaiya, A. Activation Functions In Neural Networks. *Int. J. Eng. Appl. Sci. Technol.* **2020**, *4*, 310–316. [[CrossRef](#)]
48. Spangelo, S.C.; Gilbert, E.G.; Klesh, A.T.; Kabamba, P.T.; Girard, A.R. Periodic energy-optimal path planning for solar-powered aircraft. In Proceedings of the AIAA Guidance, Navigation, and Control Conference and Exhibit, Chicago, IL, USA, 10–13 August 2009. [[CrossRef](#)]
49. Janura, M.; Sidorenko, S.; Mircheski, I.; Iliev, V.; Angeleska, E. Bio-inspired kinetic structures. *Mech. Eng.-Sci. J.* **2022**, *40*, 33–42. [[CrossRef](#)]
50. Anderson, L.D., Jr. *Fundamentals of Aerodynamics*, 6th ed.; McGraw-Hill Education: New York, NY, USA, 2017.
51. Myers, D.R. *SOLAR RADIATION: Practical Modeling for Renewable Energy Applications*; CRC Press Taylor & Francis Group: Boca Raton, FL, USA, 2013; 212p. [[CrossRef](#)]
52. Wang, X.; Yang, Y.; Wu, D.; Zhang, Z.; Ma, X. Mission-oriented 3D path planning for high-altitude long-endurance solar-powered UAVs with optimal energy management. *IEEE Access* **2020**, *8*, 227629–227641. [[CrossRef](#)]

Disclaimer/Publisher’s Note: The statements, opinions and data contained in all publications are solely those of the individual author(s) and contributor(s) and not of MDPI and/or the editor(s). MDPI and/or the editor(s) disclaim responsibility for any injury to people or property resulting from any ideas, methods, instructions or products referred to in the content.